An analytical verification test for numerically simulated convective flow above a thermally heterogeneous surface

by Alan Shapiro, Evgeni Fedorovich, and Jeremy A. Gibbs

Abstract. An analytical solution of the Boussinesq equations for the motion of a viscous stably stratified fluid driven by a surface thermal forcing with large horizontal gradients (step changes) is obtained. This analytical solution is one of the few available for wall-bounded buoyancy-driven flows. The solution can be used to verify that computer codes for Boussinesq fluid system simulations are free of errors in formulation of wall boundary conditions and to evaluate the relative performances of competing numerical algorithms. Because the solution pertains to flows driven by a surface thermal forcing, one of its main applications may be for testing the no-slip, impermeable wall boundary conditions for the pressure Poisson equation. Examples of such tests are presented.

1 Introduction

Thermal disturbances associated with variations in underlying surface properties can drive local circulations in the atmospheric boundary layer (Atkinson, 1981; Briggs, 1988; Hadfield et al., 1991; Segal and Arritt, 1992; Simpson, 1994; Mahrt et al., 1994; Pielke, 2001; McPherson, 2007; Kang et al., 2012) and affect the development of the convective boundary layer (Patton et al., 2005; van Heerwaarden et al., 2014). Computational fluid dynamics (CFD) codes for modeling such flows commonly solve the Boussinesq equations of motion and thermal energy for a viscous/diffusive stably stratified fluid. In this paper we present an analytical solution of the Boussinesq equations for flows driven by a surface thermal forcing with large gradients (step changes) in the horizontal. The solution can be used to verify that CFD codes for Boussinesq fluid system simulations are free of errors, and to evaluate the relative performances of competing numerical algorithms. Such verification procedures are important in the development of CFD models designed for research, operational, and classroom applications.

We solve the linearized Navier-Stokes and thermal energy equations analytically for the case where the surface buoyancy varies laterally as a square wave (Fig. 1). Attention is restricted to the steady state. No boundary-layer approximations are made; the solution is non-hydrostatic, and both horizontal and vertical derivatives are included in the viscous stress and thermal diffusion terms. The solution is similar to that of Axelsen et al. (2010) for katabatic flow above a cold strip, but is easier to evaluate (no

slope present) and applies to the more general scenario where the viscosity and diffusivity coefficients can differ. The flow is also similar to a special case (no slope) considered by Egger (1981), although a final analytical solution was not provided in that study. Strictly speaking, the linearized Navier-Stokes equations apply to a class of very low Reynolds number motions known as creeping flows. Such flows appear in studies of lubrication, locomotion of microorganisms, lava flow, and flow in porous media. Of course, for the task at hand, if our linear solution is to serve as a benchmark for a nonlinear numerical model solution, it is essential that the parameter space be restricted to values for which the model's nonlinear terms are negligible.

Because the solution pertains to flows driven by a surface thermal forcing, one of its main applications may be as a test for surface boundary conditions in the pressure Poisson equation. In models of atmospheric boundary-layer flows, the buoyancy is a major contributor to the forcing term in the Poisson equation and also appears in the associated surface boundary condition. The pressure boundary condition on a solid boundary in incompressible (Boussinesq) fluid flows is an important and complex issue that has long been fraught with technical difficulties and controversies (Strikwerda, 1984; Orszag et al., 1986; Gresho and Sani, 1987; Gresho, 1990; Temam, 1991; Henshaw, 1994; Petersson, 2001; Sani et al., 2006; Rempfer, 2006; Guermond et al., 2006; Nordström et al., 2007; Shirokoff and Rosales, 2011; Hosseini and Feng, 2011; Vreman, 2014). Typical fractional-step solution methodologies and associated pressure (or

55 pseudo-pressure) boundary-condition implementations are often verified using various
56 prototypic flows such as Poiseuille flows, lid-driven cavity flows, flows over cylinders or
57 bluff bodies, viscously decaying vortices, and dam-break flows. We are unaware of
58 verification tests in which flows were driven by a heterogeneous surface buoyancy
59 forcing. Our solution is designed to fill this gap.

60 The analytical solution is derived in Sect. 2. In Sect. 3, this solution is compared
61 to numerically simulated fields in a steady state. Two versions of a numerical code are
62 run: a version in which the correct surface pressure boundary condition is applied, and a
63 version in which the pressure condition is mis-specified. A summary follows in Sect. 4.

64

65 **2 Analytical solution**

66 We derive the solution for steady flow over an underlying surface along which the
67 buoyancy varies laterally as a single harmonic function. This single-harmonic solution is
68 then used as a building block in a Fourier representation of the square-wave solution.

69

70 **2.1 Governing equations**

71 Consider the flow of a viscous stably stratified fluid that fills the semi-infinite domain
72 above a solid horizontal surface (placed at $z = 0$). This surface undergoes a steady
73 thermal forcing that varies periodically in the right-hand Cartesian x direction, but is
74 independent of the y direction. The two-dimensional (x, z) flow is periodic in x, and

75 satisfies the linearized (assuming the disturbance is of small amplitude) governing
76 equations under the Boussinesq approximation,

77 $$0 = -\frac{\partial \Pi}{\partial x} + \nu \nabla^2 u \,, \tag{2.1}$$

78 $$0 = -\frac{\partial \Pi}{\partial z} + b + \nu \nabla^2 w \,, \tag{2.2}$$

79 $$0 = -N^2 w + \alpha \nabla^2 b \,, \tag{2.3}$$

80 $$\frac{\partial u}{\partial x} + \frac{\partial w}{\partial z} = 0 \,. \tag{2.4}$$

81 Apart from notational differences, (2.1)–(2.4) are the two-dimensional steady state
82 versions of (55)–(57) of Sect. II of Chandrasekhar (1961). Equations (2.1) and (2.2) are
83 the horizontal (x) and vertical (z) equations of motion, respectively, (2.3) is the thermal
84 energy equation (differential form of the first law of thermodynamics) expressed in
85 terms of the buoyancy variable (defined below), and (2.4) is the incompressibility
86 condition. Here u and w are the horizontal and vertical velocity components, $\Pi \equiv$
87 $[p - p_e(z)]/\rho_w$ is the kinematic pressure perturbation [p is pressure, $p_e(z)$ is pressure in a
88 hydrostatic environmental state in which the density profile is $\rho_e(z)$, ρ_w is a constant
89 reference density, say, $\rho_e(0)$], and $b \equiv -g[\rho - \rho_e(z)]/\rho_w$ is the buoyancy, where ρ is the
90 actual density, and g is the acceleration due to gravity. The Brunt-Väisälä frequency
91 $N \equiv \sqrt{-(g/\rho_w) d\rho_e/dz}$ of the ambient fluid (Kundu 1990), kinematic viscosity ν, and
92 thermal diffusivity α are taken constant.

We obtain our solution using a standard vorticity/streamfunction formulation. Cross-differentiating (2.1) and (2.2) yields the vorticity equation,

$$0 = -\frac{\partial b}{\partial x} + \nu \nabla^2 \eta \,, \tag{2.5}$$

where $\eta \equiv \partial u/\partial z - \partial w/\partial x$ is the vorticity. Eliminating b from (2.3) and (2.5) yields

$$\nabla^4 \eta = \frac{N^2}{\nu \alpha} \frac{\partial w}{\partial x} \,. \tag{2.6}$$

Introducing a streamfunction ψ defined through

$$u = \partial \psi / \partial z, \qquad w = -\partial \psi / \partial x \,, \tag{2.7}$$

guarantees that (2.4) is satisfied, and transforms (2.6) into a single equation for ψ,

$$\nabla^6 \psi + \frac{N^2}{\nu \alpha} \frac{\partial^2 \psi}{\partial x^2} = 0 \,. \tag{2.8}$$

The dependent variables are assumed to vanish far above the surface ($z \to \infty$). On the surface we apply no-slip ($u = 0$) and impermeability ($w = 0$) conditions, and specify a periodic (in x) buoyancy distribution. As we will now see, restricting the dependent variables to steady periodic forms that vanish as $z \to \infty$ also restricts acceptable distributions of the surface buoyancy. The restriction was first noted by Egger (1981, Sect. 3c), though without details. Averaging (2.3) over one period (using $w = -\partial \psi / \partial x$) yields $d^2 \overline{b}/dz^2 = 0$, which integrates to $\overline{b} = A + B z$ ($\overline{b}$ is the average of b; A and B are constants). Taking $b \to 0$ as $z \to \infty$, implies that $\overline{b} \to 0$ as $z \to \infty$, in which case $A = B = 0$, and $\overline{b}(z) = 0$. In particular, at the surface, $\overline{b}(0) = 0$. If a surface distribution

111 $b(x,0)$ violates this condition, the ground acts as a net heat source/sink. In an unsteady
112 model, such a source/sink would force a continually upward-developing disturbance, and
113 a steady state could never be attained.
114
115 **2.2 Single-harmonic forcing**
116 For a surface buoyancy of the form $b(x,0) \propto \sin kx$, (2.3) indicates that ψ is of the form
117 $$\psi = A(z)\cos kx\,. \tag{2.9}$$
118 Application of (2.9) in (2.8) yields
119 $$\left(\frac{d^2}{dz^2} - k^2\right)^3 A - \frac{N^2k^2}{\nu\alpha}A = 0\,, \tag{2.10}$$
120 which has solutions of the form $A \propto e^{Mz}$ for M satisfying
121 $$(M^2 - k^2)^3 = \frac{N^2k^2}{\nu\alpha}\,. \tag{2.11}$$
122 Taking the one-third power of (2.11) yields a useful intermediate result:
123 $$M^2 - k^2 = \frac{N^{2/3}k^{2/3}}{\nu^{1/3}\alpha^{1/3}}e^{2n\pi i/3}\,, \tag{2.12}$$
124 where n is an integer. Rearranging (2.12) and taking the square root yields
125 $$M = \pm\sqrt{k^2 + \frac{N^{2/3}k^{2/3}}{\nu^{1/3}\alpha^{1/3}}e^{2n\pi i/3}}\,. \tag{2.13}$$
126 Equation (2.13) furnishes six roots, two for each of $n = 0$, 1, 2. To ensure that $A(z) \to 0$
127 as $z \to \infty$, we reject the roots with a positive real part. With the radicand of (2.13)

expressed in polar form, the physically acceptable roots are

$$M_0 = -\sqrt{k^2 + \frac{N^{2/3}k^{2/3}}{\nu^{1/3}\alpha^{1/3}}}\,, \quad (n=0), \tag{2.14a}$$

$$M_1 = -r^{1/2}e^{i\phi/2}, \qquad (n=1), \tag{2.14b}$$

$$M_2 = -r^{1/2}e^{-i\phi/2}\,, \qquad (n=2), \tag{2.14c}$$

where the subscript on M denotes the associated value of n, and r and ϕ are defined by

$$r \equiv \sqrt{\left[k^2 + \frac{N^{2/3}k^{2/3}}{\nu^{1/3}\alpha^{1/3}}\cos\left(\frac{2\pi}{3}\right)\right]^2 + \left[\frac{N^{2/3}k^{2/3}}{\nu^{1/3}\alpha^{1/3}}\sin\left(\frac{2\pi}{3}\right)\right]^2}\,, \tag{2.15}$$

$$\cos\phi = \frac{1}{r}\left[k^2 + \frac{N^{2/3}k^{2/3}}{\nu^{1/3}\alpha^{1/3}}\cos\left(\frac{2\pi}{3}\right)\right], \qquad \sin\phi = \frac{1}{r}\left(\frac{N^{2/3}k^{2/3}}{\nu^{1/3}\alpha^{1/3}}\right)\sin\left(\frac{2\pi}{3}\right) > 0\,. \tag{2.16}$$

While solving (2.16) for ϕ, care must be taken when evaluating arcsin or arccos functions that ϕ appears in the correct quadrant (ϕ should be in quadrant I or II so $\phi/2$ should always be in quadrant I). Also note from (2.14b) and (2.14c) that M_2 is the complex conjugate of M_1 ($M_2 = M_1{}^*$), a fact that will often be used below.

With the general solution for ψ written as

$$\psi = (B\,e^{M_0 z} + Ce^{M_1 z} + De^{M_2 z})\cos kx\,, \tag{2.17}$$

where B, C, and D are constants, the vorticity becomes,

$$\eta = \left[B(M_0^2 - k^2)\,e^{M_0 z} + C(M_1^2 - k^2)e^{M_1 z} + D(M_2^2 - k^2)e^{M_2 z}\right]\cos kx\,, \tag{2.18}$$

and the buoyancy follows from (2.3) as

$$b = \frac{kN^2}{\alpha}\left(\frac{B}{M_0^2 - k^2}e^{M_0 z} + \frac{C}{M_1^2 - k^2}e^{M_1 z} + \frac{D}{M_2^2 - k^2}e^{M_2 z}\right)\sin kx + b_h\,, \tag{2.19}$$

where $\nabla^2 b_h = 0$. In view of (2.12), equation (2.19) becomes

$$b = \frac{k^{1/3}\nu^{1/3}N^{4/3}}{\alpha^{2/3}}(B\,e^{M_0 z} + e^{-2\pi i/3}\,C\,e^{M_1 z} + e^{-4\pi i/3}\,D\,e^{M_2 z})\sin kx + b_h\,. \tag{2.20}$$

Applying (2.18) and (2.20) in (2.5) yields an equation for $\partial b_h/\partial x$, which upon use of (2.12) and $M_2 = M_1{}^*$ reduces to $\partial b_h/\partial x = 0$. So b_h is, at most, a function of z. Since $\nabla^2 b_h = 0$, b_h is, at most, a linear function of z, and since b should vanish as $z \to \infty$, that linear function must be 0. Thus, $b_h = 0$.

The pressure follows from (2.1) and (2.12) as

$$\Pi = \frac{\nu^{2/3}N^{2/3}}{k^{1/3}\alpha^{1/3}}\,(BM_0\,e^{M_0 z} + CM_1 e^{2\pi i/3}e^{M_1 z} + DM_2 e^{4\pi i/3}e^{M_2 z})\sin kx + G(z)\,, \tag{2.21}$$

where $G(z)$ is a function of integration. Applying (2.21) in (2.2), and using (2.11) yields $dG/dz = 0$, so G is constant. For Π to vanish as $z \to \infty$, this constant must be zero.

The surface conditions determine B, C, and D. The surface buoyancy is

$$b(x,0) = b_0 \sin kx\,, \tag{2.22}$$

where b_0 is a constant forcing amplitude. Application of (2.20) in (2.22) yields

$$B + e^{-2\pi i/3}\,C + e^{-4\pi i/3}\,D = \frac{b_0\alpha^{2/3}}{k^{1/3}\nu^{1/3}N^{4/3}}\,. \tag{2.23}$$

In view of (2.7) and (2.17), the impermeability condition $w(x,0) = 0$ and no-slip

condition $u(x,0) = 0$ yield

$$B + C + D = 0\,, \tag{2.24}$$

$$BM_0 + CM_1 + DM_2 = 0\,. \tag{2.25}$$

Straightforward but lengthy manipulations yield the solution of (2.23)–(2.25):

$$B = -\left(\frac{b_0\,\alpha^{2/3}}{\sqrt{3}\,k^{1/3}\nu^{1/3}N^{4/3}}\right)\frac{2r^{1/2}\sin(\phi/2)}{M_0 + 2r^{1/2}\cos(\pi/3+\phi/2)}\,, \tag{2.26}$$

$$C = -i\left(\frac{b_0\,\alpha^{2/3}}{\sqrt{3}\,k^{1/3}\nu^{1/3}N^{4/3}}\right)\frac{M_2 - M_0}{M_0 + 2r^{1/2}\cos(\pi/3+\phi/2)}\,, \tag{2.27}$$

$$D = i\left(\frac{b_0\,\alpha^{2/3}}{\sqrt{3}\,k^{1/3}\nu^{1/3}N^{4/3}}\right)\frac{M_1 - M_0}{M_0 + 2r^{1/2}\cos(\pi/3+\phi/2)}\,. \tag{2.28}$$

Applying (2.26)–(2.28) in (2.17), (2.20), and (2.18), with (2.12) used in the latter equation, and noting that B is real, while $D = C^*$ (since $M_2 = M_1{}^*$), we obtain

$$b = \frac{2b_0}{\sqrt{3}}\,\frac{e^{-Z_c}[\mu\cos(Z_s+\pi/6) + \cos(Z_s+\pi/6+\phi/2)] - e^{M_0 z}\sin(\phi/2)}{\mu + 2\cos(\pi/3+\phi/2)}\sin kx\,, \tag{2.29}$$

$$\psi = \frac{2b_0\,\alpha^{2/3}}{\sqrt{3}\,k^{1/3}\nu^{1/3}N^{4/3}}\,\frac{e^{-Z_c}[\mu\sin Z_s + \sin(Z_s+\phi/2)] - e^{M_0 z}\sin(\phi/2)}{\mu + 2\cos(\pi/3+\phi/2)}\cos kx\,, \tag{2.30}$$

where

$$Z_s \equiv z\,r^{1/2}\sin(\phi/2), \quad Z_c \equiv z\,r^{1/2}\cos(\phi/2), \quad \mu \equiv M_0/r^{1/2}\,. \tag{2.31}$$

Application of (2.30) in (2.7) yields the velocity components as

$$u = \frac{2b_0\,\alpha^{2/3} r^{1/2}}{\sqrt{3}\,k^{1/3}\nu^{1/3}N^{4/3}}\;\frac{e^{-Z_c}[\mu\sin(\phi/2 - Z_s) - \sin Z_s] - \mu e^{M_0 z}\sin(\phi/2)}{\mu + 2\cos(\pi/3 + \phi/2)}\cos kx \tag{2.32}$$

$$w = \frac{2b_0\,\alpha^{2/3} k^{2/3}}{\sqrt{3}\,\nu^{1/3}N^{4/3}}\;\frac{e^{-Z_c}[\mu\sin Z_s + \sin(Z_s + \phi/2)] - e^{M_0 z}\sin(\phi/2)}{\mu + 2\cos(\pi/3 + \phi/2)}\sin kx\,. \tag{2.33}$$

2.3 Piecewise constant (square wave) forcing

Next, consider the case where the surface buoyancy varies horizontally as a square wave, with a distribution over one period L given by

$$b(x,0) = \begin{cases} b_{\max}, & 0 < x < L/2, \\ -b_{\max}, & L/2 < x < L. \end{cases} \tag{2.34}$$

Such a distribution can be expressed as the Fourier series:

$$b(x,0) = \sum_{n=1}^{\infty} b_n \sin\left(\frac{n\pi x}{L}\right), \tag{2.35}$$

$$b_n = \frac{2}{L}\int_0^L b(x,0)\sin\left(\frac{n\pi x}{L}\right). \tag{2.36}$$

Application of (2.34) in (2.36) yields

$$b_n = \frac{2b_{\max}}{n\,\pi}\big[1 - 2\cos(n\,\pi/2) + \cos(n\,\pi)\big]. \tag{2.37}$$

The solutions for b, ψ, u, and w can then be written as summations over the single-harmonic solutions (2.29), (2.30), (2.32), and (2.33), with k related to n by

$$k = \frac{n\,\pi}{L}\,, \tag{2.38}$$

and with b_0 replaced by b_n:

$$b = \frac{2}{\sqrt{3}} \sum_{n=1}^{\infty} b_n \frac{e^{-Z_c}[\mu \cos(Z_s + \pi/6) + \cos(Z_s + \pi/6 + \phi/2)] - e^{M_0 z} \sin(\phi/2)}{\mu + 2\cos(\pi/3 + \phi/2)} \sin\left(\frac{n\pi x}{L}\right), \quad (2.39)$$

$$\psi = \frac{2\,\alpha^{2/3}}{\sqrt{3}\,\nu^{1/3} N^{4/3}} \sum_{n=1}^{\infty} \frac{b_n}{k^{1/3}} \frac{e^{-Z_c}[\mu \sin Z_s + \sin(Z_s + \phi/2)] - e^{M_0 z} \sin(\phi/2)}{\mu + 2\cos(\pi/3 + \phi/2)} \cos\left(\frac{n\pi x}{L}\right), \quad (2.40)$$

$$u = \frac{2\,\alpha^{2/3}}{\sqrt{3}\,\nu^{1/3} N^{4/3}} \sum_{n=1}^{\infty} b_n \frac{r^{1/2}}{k^{1/3}} \frac{e^{-Z_c}[\mu \sin(\phi/2 - Z_s) - \sin Z_s] - \mu e^{M_0 z} \sin(\phi/2)}{\mu + 2\cos(\pi/3 + \phi/2)} \cos\left(\frac{n\pi x}{L}\right), \quad (2.41)$$

$$w = \frac{2\,\alpha^{2/3}}{\sqrt{3}\,\nu^{1/3} N^{4/3}} \sum_{n=1}^{\infty} b_n k^{2/3} \frac{e^{-Z_c}[\mu \sin Z_s + \sin(Z_s + \phi/2)] - e^{M_0 z} \sin(\phi/2)}{\mu + 2\cos(\pi/3 + \phi/2)} \sin\left(\frac{n\pi x}{L}\right). \quad (2.42)$$

3 Verification tests

A solution of the linearized equations may be used to verify a nonlinear code if the nonlinear terms are sufficiently small. Unfortunately, *a priori* estimates of such terms expressed, for example, through a Reynolds number, are not straightforward since the relevant velocity and length scales in our problem are only evident after a solution has been obtained. We thus seek an appropriate set of test parameters through trial and error, guided by *a posteriori* linear solution estimates of the terms $\mathbf{u} \cdot \nabla b$ and $\mathbf{u} \cdot \nabla \eta$ $[\mathbf{u} = (u, w)]$ present in nonlinear versions of (2.3) and (2.5), respectively. Specifically, for any computed candidate solution, we formed the ratios of the largest values of those nonlinear terms to the largest values of the corresponding linear terms, that is, the

205 terms actually present in (2.3) and (2.5). We need only consider one such linear term
206 per ratio since (2.3) and (2.5) are comprised of two terms of equal magnitude. A
207 solution was deemed to be sufficiently linear if

208 $$R_\eta \equiv \frac{\max\left|\mathbf{u}\cdot\nabla\eta\right|}{\max\left|\partial b/\partial x\right|} < \varepsilon, \quad \text{and} \quad R_b \equiv \frac{\max\left|\mathbf{u}\cdot\nabla b\right|}{\max\left|\alpha\nabla^2 b\right|} < \varepsilon\,, \tag{3.1}$$

209 where ε ($<<$ 1) is a prescribed threshold. The suitability of this approach was
210 confirmed by the very close agreement between the analytical solutions and the
211 numerical solutions obtained with the correct surface pressure condition.

212 The numerical model employed in our tests is a variant of a direct numerical
213 simulation (DNS) code used in the boundary-layer and slope-flow studies of Fedorovich
214 et al. (2001), Fedorovich and Shapiro (2009a,b), and Shapiro and Fedorovich (2013,
215 2014). The model solves the Boussinesq governing equations on a staggered (Arakawa
216 C) grid. Although designed for three-dimensional simulations, the model was run in a
217 two-dimensional (x, z) mode. The overall solution procedure is patterned on a fractional
218 step method proposed by Chorin (1968). In our version, the prognostic equations are
219 integrated using a filtered leapfrog scheme with explicit treatment of the viscous term.
220 The pressure is diagnosed from a Poisson equation (equation (A3b), discussed in the
221 Appendix), which is solved using a fast Fourier transform technique in horizontal
222 planes, and a tridiagonal matrix inversion in the vertical. The surface condition on
223 pressure is the inhomogeneous Neumann condition (INC) that arises from projecting the

vertical equation of motion into the vertical, and imposing the impermeability condition (Vreman, 2014; also see the Appendix). We also run a version of the code in which the surface pressure condition is mis-specified as a homogeneous Neumann condition (HNC). We hasten to add, however, that our implementation of the HNC may be quite different from implementations described in the literature. We elaborate on these technical differences and review general aspects of the problem of surface pressure specification in the Appendix.

The analytical solution was evaluated on an un-staggered (x, z) grid extending over one period of the square wave ($x = 0$ to $x = L$). The series were truncated at 50000 terms. The governing parameters were adjusted so that the linearity criteria were satisfied in comparisons with $\varepsilon = 5\times10^{-3}$.

In the first test, we set $\nu = \alpha = 0.001\,\mathrm{m^2\,s^{-1}}$, $N = 0.02\,\mathrm{s^{-1}}$, $L = 5.12\,\mathrm{m}$, and $b_{\max}$ $= 1\times10^{-5}\mathrm{m\,s^{-2}}$. For the analytical solution A-1, the (x, z) grid consisted of 513 points in the x direction and 1025 points in the z direction, with grid spacings $\Delta x = \Delta z = 0.01\,\mathrm{m}$. The linearity criteria (3.1) were satisfied with $R_\eta \cong 8.2\times10^{-5}$ and $R_b \cong 2.8\times10^{-3}$. The analytical b and w fields shown in Fig. 2 depict a broad zone of ascent above the warm surface and a compensating zone of descent over the cold surface, roughly for $z < 1.8\,\mathrm{m}$. In the upper part of these zones (at roughly $0.9\,\mathrm{m} < z < 1.8\,\mathrm{m}$), adiabatic expansion/compression has reversed the senses of the

243 buoyancy fields. Surprisingly, the numerical fields in the inhomogeneous INC-1 and
244 homogeneous HNC-1 cases are very similar to each other and to the A-1 fields. The u
245 fields from A-1, INC-1, and HNC-1 shown in Fig. 3 are visually indistinguishable from
246 one another.

247 To understand why the INC-1 and HNC-1 simulations are so similar, and to
248 identify simulation parameters that might evince more substantial differences, we
249 consider the idealized problem in which a specified buoyancy $b = b_0 e^{-\gamma z}\sin kx$ ($\gamma = h^{-1}$,
250 where h is the e-folding depth scale) is the only forcing term in the Poisson equation
251 $\nabla^2\Pi = \partial b/\partial z$, with Neumann surface condition $\partial\Pi/\partial z\big|_0 = b(x,0)$. This idealized
252 problem is solved as

253 $$\Pi^*_{\mathrm{INC}} = \frac{b_0}{\gamma^2 - k^2}\left(k\,e^{-kz} - \gamma\,e^{-\gamma z}\right)\sin kx\,. \tag{3.2}$$

254 The corresponding solution obtained with the homogeneous Neumann condition,
255 $\partial\Pi/\partial z\big|_0 = 0$, is

256 $$\Pi^*_{\mathrm{HNC}} = \frac{b_0}{\gamma^2 - k^2}\left(\frac{\gamma^2}{k}\,e^{-kz} - \gamma\,e^{-\gamma z}\right)\sin kx\,. \tag{3.3}$$

257 The relative error (RE) in the vertical pressure gradient force associated with (3.2) and
258 (3.3), defined as the local absolute error in that force divided by the local buoyancy, is
259 calculated as

$$RE \equiv \left| \frac{\partial \Pi^*_{\mathrm{INC}}/\partial z - \partial \Pi^*_{\mathrm{HNC}}/\partial z}{b} \right| = e^{(a-1)kz}, \tag{3.4}$$

where $a \equiv \gamma/k$. Written in terms of the depth scale h and wavelength $\lambda = 2\pi/k$, a can be interpreted as an aspect ratio characterizing the width to depth scales of the disturbance, $a = \lambda/(2\pi h) \propto \lambda\gamma$. From (3.4) we see that RE decreases exponentially with z for disturbances characterized by small aspect ratios, $a < 1$ (which we refer to as deep disturbances) and increases exponentially with z for disturbances characterized by large aspect ratios, $a > 1$ (which we refer to as shallow disturbances). The buoyancy in Fig. 2 is suggestive of $a < 1$, which indicates that the first test could be classified as a deep (error-forgiving) simulation.

The preceding analysis suggests that simulations with shallow thermal disturbances ($a > 1$) might yield large differences between cases with inhomogeneous and homogeneous Neumann conditions. There did not appear to be a straightforward way to increase the effective a by systematically varying the parameters (e.g., increasing L tended to increase the effective h), but a set of suitable parameters were identified through trial and error and were used as the basis for the second test case.

In the second test, we set $\nu = \alpha = 0.0001\,\mathrm{m^2 s^{-1}}$, $N = 0.2\,\mathrm{s^{-1}}$, $L = 10.24\,\mathrm{m}$, and $b_{\max} = 5\times10^{-6}\,\mathrm{ms^{-2}}$. The analytical solution A-2 was generated with 2049 points in the x direction and 513 points in the z direction, with grid spacings of $\Delta x = \Delta z = 0.005\,\mathrm{m}$. The linearity criteria were satisfied with $R_\eta \cong 4.8\times10^{-5}$ and $R_b \cong 3.8\times10^{-3}$. In

279 contrast to the counter-rotating convection rolls seen in the first test, the analytical b
280 and w fields shown in Fig. 4 depict narrow updraft/downdraft pairs straddling the
281 buoyancy discontinuities. Between the narrow updrafts is a broad region of relatively
282 weak ascent. The w and b fields above the cold surface are mirror images of the fields
283 above the warm surface. Note the change in the scales of the x and (especially) the z
284 axes between Figs. 4 and 2: the low-level thermal disturbance in the second test is much
285 shallower than the disturbance in the first test (and is suggestive of $a > 1$). In this
286 second test case we find dramatic differences between the inhomogeneous INC-2 and
287 homogeneous HNC-2 cases. Specifically, while the INC-2 and A-2 fields are in excellent
288 agreement, the HNC-2 fields showed no signs of even approaching a steady state. Long
289 after the INC-2 simulation had reached a steady state, the HNC-2 fields continued to
290 amplify and develop asymmetric structures associated with flow nonlinearities. The very
291 close agreement between the A-2 solution and the steady state in the INC-2 simulation
292 is shown for the u field in Fig. 5. The u field in the disastrous HNC-2 simulation, at a
293 time when a steady state had already been attained in the INC-2 simulation, is shown
294 in Fig. 6.
295
296 **4 Summary**
297 The linearized Boussinesq equations for the motion of a viscous stably stratified fluid
298 are solved analytically for a surface buoyancy that varies laterally as a square wave.

299 The solution describes two-dimensional laminar convective structures such as thermal
300 convective rolls and updraft/downdraft pairs. The main applications of the solution may
301 be in code verification and the evaluation of different implementations of the surface
302 pressure condition for the pressure Poisson equation. Tests have been conducted for
303 cases where the aspect ratios of the thermal disturbance have been large and small.
304 With attention restricted to disturbances of sufficiently small amplitude, the linear
305 solution and numerically simulated fields with the inhomogeneous Neumann condition
306 for pressure (which is appropriate in the context of the particular fractional step
307 procedure adopted in our DNS code) have been found to be in excellent agreement for
308 both tests. However, in tests with a mis-specified Neumann condition, an excellent
309 agreement with the analytical solution has been found only for the deep (small aspect
310 ratio) disturbance case; errors in the shallow (large aspect ratio) disturbance case have
311 been catastrophic.

Appendix A: Comment on the pressure condition at a lower solid surface

Consider a three-dimensional Boussinesq system with equation of motion,

$$\frac{\partial \mathbf{u}}{\partial t} = -\nabla \Pi + \nu \nabla^2 \mathbf{u} + \mathbf{F} \,. \tag{A1}$$

Here $\mathbf{u} = (u, v, w)$ is the three-dimensional velocity vector, Π is a kinematic pressure perturbation, ν is the kinematic viscosity coefficient, and $\mathbf{F}$ is the sum of nonlinear acceleration and buoyancy terms. Applying the incompressibility condition,

$$\nabla \cdot \mathbf{u} = 0 \,, \tag{A2}$$

in the equation that results from taking the divergence of (A1) (e.g., Orszag et al., 1986) yields the Poisson equation,

$$\nabla^2 \Pi = \nabla \cdot \mathbf{F} \,. \tag{A3a}$$

Although (A1) and (A2) imply (A3a), the reverse statement is not generally true. Indeed, eliminating Π from between (A3a) and the equation arising from taking the divergence of (A1) yields the diffusion equation $\partial \delta / \partial t = \nu \nabla^2 \delta$ for the velocity divergence $\delta \equiv \nabla \cdot \mathbf{u}$, whose solution is (A2) only if δ is zero initially and on all boundaries (Orszag et al., 1986; Gresho and Sani, 1987, Vreman 2014).

The same steps leading to (A3a) also lead to an alternative Poisson equation,

$$\nabla^2 \Pi = \nabla \cdot \Big(\nu \nabla^2 \mathbf{u} + \mathbf{F} \Big) . \tag{A3b}$$

Although $\nabla \cdot \nu \nabla^2 \mathbf{u}$ was omitted in (A3a) [this term is zero if (A2) is satisfied], without further constraints on δ (described above), (A2) may not be satisfied. Gresho and Sani

(1987) showed that the retention of $\nabla \cdot \nu \nabla^2 \mathbf{u}$ in (A3b) assures that (A2) is satisfied, and thus leads to the paradox: "If you include it, you don't need it; if you don't include it, you need it." Vreman (2014) revisited this paradox, and showed that for a standard staggered method, the discretized form of (A3b) is equivalent to that of (A3a) supplemented with the constraint that $\nabla \cdot \nabla^2 \mathbf{u} = 0$ $(\nabla^2 \delta = 0)$ on points adjacent to the solid boundary [with the same inhomogeneous Neumann boundary condition for Π implied for (A3a) and (A3b)]. When supplemented with this $\nabla^2 \delta = 0$ near-wall condition, the diffusion equation for δ led to $\delta = 0$ for all time. We note that (A3b) is the form adopted in our numerical code.

Evaluating the vertical component of (A1) on the surface, where the impermeability condition applies, yields the inhomogeneous Neumann condition,

$$\left.\frac{\partial \Pi}{\partial z}\right|_0 = \nu \left.\frac{\partial^2 w}{\partial z^2}\right|_0 + F_z\Big|_0 , \tag{A4}$$

where $w \equiv \mathbf{k} \cdot \mathbf{u}$, $F_z \equiv \mathbf{k} \cdot \mathbf{F}$, $\mathbf{k}$ is the upward unit vector, and $(\,)\big|_0$ is a surface value. It has been argued that (A4), by itself, is not a proper boundary condition because it does not provide new information (it is not independent of the governing equations) and does not enforce the incompressibility condition (A2) at the boundary (Strikwerda, 1984; Henshaw, 1994; Sani et al., 2006). However, as pointed out by Henshaw (1994), many studies that impose (A4) (or a variant of it) also apply (A2) on the boundary.

In our numerical model, (A1) is integrated using a fractional step procedure with

explicit treatment of the viscous term. First, a provisional velocity field $\tilde{\mathbf{u}}$ that does not satisfy (A2) is obtained by integrating a discretized form of (A1) in which the pressure gradient is omitted. The provisional velocity is equal to the velocity at the end of the previous time step plus the sum of the forcing terms (nonlinear acceleration, buoyancy, and viscous stress) multiplied by the time step Δt. With the forcing terms explicitly evaluated, $\tilde{\mathbf{u}}$ is readily computed throughout the flow domain, including on the surface, where, in surface-forced flows, the buoyancy will make a substantial contribution. In terms of $\tilde{\mathbf{u}}$ and its vertical component $\tilde{w}$, (A3b) and (A4) become,

$$\nabla^2 \Pi = \frac{\nabla \cdot \tilde{\mathbf{u}}}{\Delta t}, \tag{A5}$$

$$\left.\frac{\partial \Pi}{\partial z}\right|_0 - \frac{1}{\Delta t}\tilde{w}\Big|_0 = 0\,. \tag{A6}$$

In the second step, a velocity field that does satisfy (A2) is obtained by solving (A5) for Π and then adding the pressure gradient force associated with Π (multiplied by Δt) to $\tilde{\mathbf{u}}$.

In some explicit fractional step procedures (including the DNS code used in our study), the problem of solving (A5) subject to (A6) with $\tilde{\mathbf{u}}\big|_0$ evaluated from model data is replaced by what appears to be an entirely different (but is actually equivalent) problem: solving (A5) subject to the homogeneous Neumann condition,

$$\left.\frac{\partial \Pi}{\partial z}\right|_0 = 0, \tag{A7}$$

in concert with $\tilde{\mathbf{u}}\big|_0$ being set to 0, obviating the need to calculate $\tilde{\mathbf{u}}\big|_0$ from model data. It can be shown that $\tilde{w}\big|_0$ and the discretized form of $\partial\Pi/\partial z\big|_0$ appear in the discretized form of (A5) valid half a grid point above the physical surface as $\partial\Pi/\partial z\big|_0 - \tilde{w}\big|_0/\Delta t$, that is, in the same combination as they appear in (A6). Thus, setting $\tilde{w}\big|_0$ and $\partial\Pi/\partial z\big|_0$ to 0, is equivalent to implementing (A6) with the model-computed values of $\tilde{w}\big|_0$: the discretized form of (A5) near the surface is the same in either case. Moreover, on the C grid, setting the tangential components $\tilde{u}\big|_0$ and $\tilde{v}\big|_0$ to 0 only affects the values of $\tilde{u}$ and $\tilde{v}$ half a grid point beneath the physical boundary. These values do not appear in the discretized form of (A5) at any z-level, and thus have no bearing on the solution. In essence, the errors associated with the conflation of the two physically unjustifiable specifications (homogeneous Neumann condition for pressure, and $\tilde{\mathbf{u}}\big|_0 = 0$) cancel out.

The homogeneous Neumann condition for pressure can be the source of confusion if the context in which the condition is applied is not made clear: it would be a correct condition if $\tilde{\mathbf{u}}\big|_0$ is set to zero (per the equivalence described above), but it would be an incorrect condition if the explicit model-computed values of $\tilde{\mathbf{u}}\big|_0$ are used. In the experiments with the mis-specified condition described in Sect. 3, the homogeneous condition is imposed in the latter context. Unfortunately, in many numerical model descriptions, the nature of the surface pressure condition is left vague, for example, by

not indicating whether a Neumann condition is homogeneous or inhomogeneous, or, if a homogeneous Neumann condition is indicated, not mentioning how $\tilde{\mathbf{u}}\big|_0$ is treated.

Finally, we note that in fractional step procedures that treat the viscous term implicitly (e.g., Kim and Moin, 1985; Gresho, 1990; Armfield and Street, 2002; Guermond et al., 2006, and many others), the homogeneous Neumann condition is often applied as a surface condition for a Poisson equation, but it is again different from our implementation described in Sect. 3. In the implicit treatments, the provisional velocity is obtained as the solution of a boundary value problem ($\tilde{\mathbf{u}}\big|_0$ should be specified; often it is set to 0) in which the relevant Poisson equation resembles (A5) but applies to a scalar function (sometimes called a pseudo-pressure) that is not the real pressure. Temam (1991) refers to this scalar as, "... a technical quantity, a mathematical auxiliary..." and advocates that it should not even be considered as an approximation of the pressure. Interestingly, in the context of implicit treatments, the homogeneous Neumann condition on the pseudo-pressure has sometimes been implicated as corrupting solution accuracy through the development of spurious numerical boundary layers adjacent to solid boundaries (Gresho, 1990; Guermond et al., 2006; Hosseini and Feng, 2011).

Code availability

The Fortran program used to generate output data files from the analytical solution is

406 available as a supplement to this article. That program (square.f) is configured for test
407 A-1, but can be easily adjusted to run test A-2 or other tests. Running square.f
408 automatically generates an output file for each dependent variable (e.g., u.dat) as well
409 as an output file (square.out) that summarizes the test parameters and gives the
410 computed values of the linearity ratios R_η and R_b defined in (3.1).

411

412 *Acknowledgements.* This research was supported by the National Science Foundation
413 under Grant AGS-1359698. Comments by Chiel van Heerwaarden, Juan Pedro Mellado,
414 Inanc Senocak, and an anonymous reviewer are gratefully acknowledged.

References

Armfield, S. and Street, R.: An analysis and comparison of the time accuracy of fractional-step methods for the Navier-Stokes equations on staggered grids. Int. J. Numer. Methods Fluids, 38, 255–282, 2002.

Atkinson, B.: Meso-scale Atmospheric Circulations. Academic Press. 495 pp., 1981.

Axelsen, S. L., Shapiro, A., and Fedorovich, E.: Analytical solution for katabatic flow induced by an isolated cold strip. Environ. Fluid Mech., 10, 387–414, 2010.

Briggs, G. A.: Surface inhomogeneity effects on convective diffusion. Boundary-Layer Meteorol., 45, 117–135, 1988.

Chandrasekhar, S.: Hydrodynamic and Hydromagnetic Stability. Oxford University Press. 652 pp., 1961.

Chorin, A. J.: Numerical solution of the Navier-Stokes equations. Math. Comput., 22, 745–762, 1968.

Egger, J.: On the linear two-dimensional theory of thermally induced slope winds. Beitr. Phys. Atmosph., 54, 465–481, 1981.

Fedorovich, E., Nieuwstadt, F. T. M., and Kaiser, R.: Numerical and laboratory study of a horizontally evolving convective boundary layer. Part I: Transition regimes and development of the mixed layer. J. Atmos. Sci., 58, 70–86, 2001.

Fedorovich, E. and Shapiro, A.: Structure of numerically simulated katabatic and anabatic flows along steep slopes. Acta Geophys., 57, 981–1010, 2009a.

435 Fedorovich, E. and Shapiro, A.: Turbulent natural convection along a vertical plate
436 immersed in a stably stratified fluid. J. Fluid Mech., 636, 41–57, 2009b.
437 Gresho, P. M. and Sani, R. L.: On pressure boundary conditions for the incompressible
438 Navier-Stokes equations. Int. J. Numer. Methods Fluids, 7, 1111–1145, 1987.
439 Gresho, P. M.: On the theory of semi-implicit projection methods for viscous
440 incompressible flow and its implementation via a finite element method that also
441 introduces a nearly consistent mass matrix. Part 1: Theory. Int. J. Numer.
442 Methods Fluids, 11, 587–620, 1990.
443 Guermond, J. L., Minev, P., and Shen, J.: An overview of projection methods for
444 incompressible flows. Comput. Methods Appl. Mech. Engrg. 195, 6011–6045,
445 2006.
446 Hadfield, M. G., Cotton, W. R., and Pielke, R. A.: Large-eddy simulations of thermally
447 forced circulations in the convective boundary layer. Part I: A small-scale
448 circulation with zero wind. Boundary-Layer Meteorol., 57, 79–114, 1991.
449 Henshaw, W. D: A fourth-order accurate method for the incompressible Navier-Stokes
450 equations on overlapping grids. J. Comput. Phys., 113, 13–25, 1994.
451 Hosseini, S. M. and Feng, J. J.: Pressure boundary conditions for computing
452 incompressible flows with SPH. J. Comput. Phys., 230, 7473–7487, 2011.
453 Kang, S.-L., Lenschow, D., and Sullivan, P.: Effects of mesoscale surface thermal
454 heterogeneity on low-level horizontal wind speeds. Boundary-Layer Meteorol.,

143, 409–432, 2012.

Kim, J. and Moin, P.: Application of a fractional-step method to incompressible Navier-Stokes equations. J. Comput. Phys., 59, 308–323, 1985.

Kundu, P. K.: Fluid Mechanics. Academic Press. 638 pp., 1990.

Mahrt, L., Sun, J., Vickers, D., MacPherson, J. I., Pederson, J. R., and Desjardins, R. L.: Observations of fluxes and inland breezes over a heterogeneous surface. J. Atmos. Sci., 51, 2484–2499, 1994.

McPherson, R. A.: A review of vegetation-atmosphere interactions and their influences on mesoscale phenomena. Prog. Phys. Geog., 31, 261–285, 2007.

Nordström, J., Mattsson, K., and Swanson, C.: Boundary conditions for a divergence free velocity-pressure formulation of the Navier-Stokes equations. J. Comput. Phys., 225, 874–890, 2007.

Orszag, S. A., Israeli, M., and Deville, M. O.: Boundary conditions for incompressible flows. J. Sci. Comput., 1, 75–111, 1986.

Patton, E. G., Sullivan, P. P., and Moeng, C.-H.: The influence of idealized heterogeneity on wet and dry planetary boundary layers coupled to the land surface. J. Atmos. Sci., 62, 2078–2097, 2005.

Petersson, N. A.: Stability of pressure boundary conditions for Stokes and Navier-Stokes equations. J. Comput. Phys., 172, 40–70, 2001.

Pielke, R. A.: Influence of the spatial distribution of vegetation and soils on the

475 prediction of cumulus convective rainfall. Rev. Geophys., 39, 151–177, 2001.
476 Rempfer, D.: On boundary conditions for incompressible Navier-Stokes problems. Appl.
477 Mech. Rev., 59, 107–125, 2006.
478 Segal, M. and Arritt, R. W.: Non-classical mesoscale circulations caused by surface
479 sensible heat-flux gradients. Bull. Amer. Meteorol. Soc., 73, 1593–1604, 1992.
480 Shirokoff, D. and Rosales, R. R.: An efficient method for the incompressible Navier-
481 Stokes equations on irregular domains with no-slip boundary conditions, high
482 order up to the boundary. J. Comput. Phys., 230, 8619–8646, 2011.
483 Shapiro, A. and Fedorovich, E.: Similarity models for unsteady free convection flows
484 along a differentially cooled horizontal surface. J. Fluid Mech., 736, 444–463,
485 2013.
486 Shapiro, A. and Fedorovich, E.: A boundary-layer scaling for turbulent katabatic flow.
487 Boundary-Layer Meteorol., 153, 1–17, 2014.
488 Simpson, J. E.: Sea Breeze and Local Winds. Cambridge University Press. 234 pp.,
489 1994.
490 Temam, R.: Remark on the pressure boundary condition for the projection method.
491 Theoret. Comput. Fluid Dynamics, 3, 181–184, 1991.
492 Strikwerda, J. C.: Finite difference methods for the Stokes and Navier-Stokes equations.
493 SIAM J. Sci. Stat. Comput., 5, 56–68, 1984.
494 van Heerwaarden, C. C., Mellado, J. P., and de Lozar, A.: Scaling laws for the

heterogeneously heated free convective boundary layer. J. Atmos. Sci., 71, 3975–4000, 2014.

Vreman, A. W.: The projection method for the incompressible Navier-Stokes equations: The pressure near a no-slip wall. J. Comput. Phys., 263, 353–374, 2014.

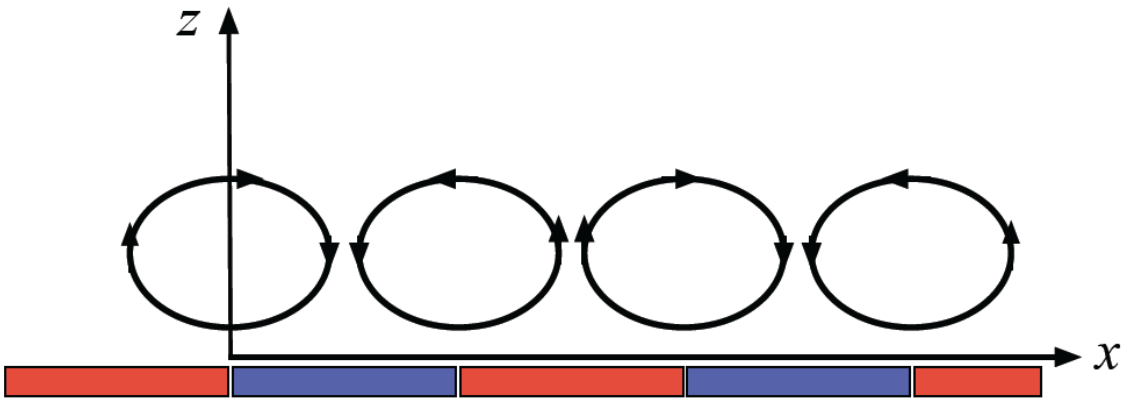

Figure 1. Schematic of two-dimensional (x, z) thermal convection induced by a surface buoyancy that varies horizontally (x) as a square wave. Red denotes positive surface buoyancy, blue denotes negative surface buoyancy.

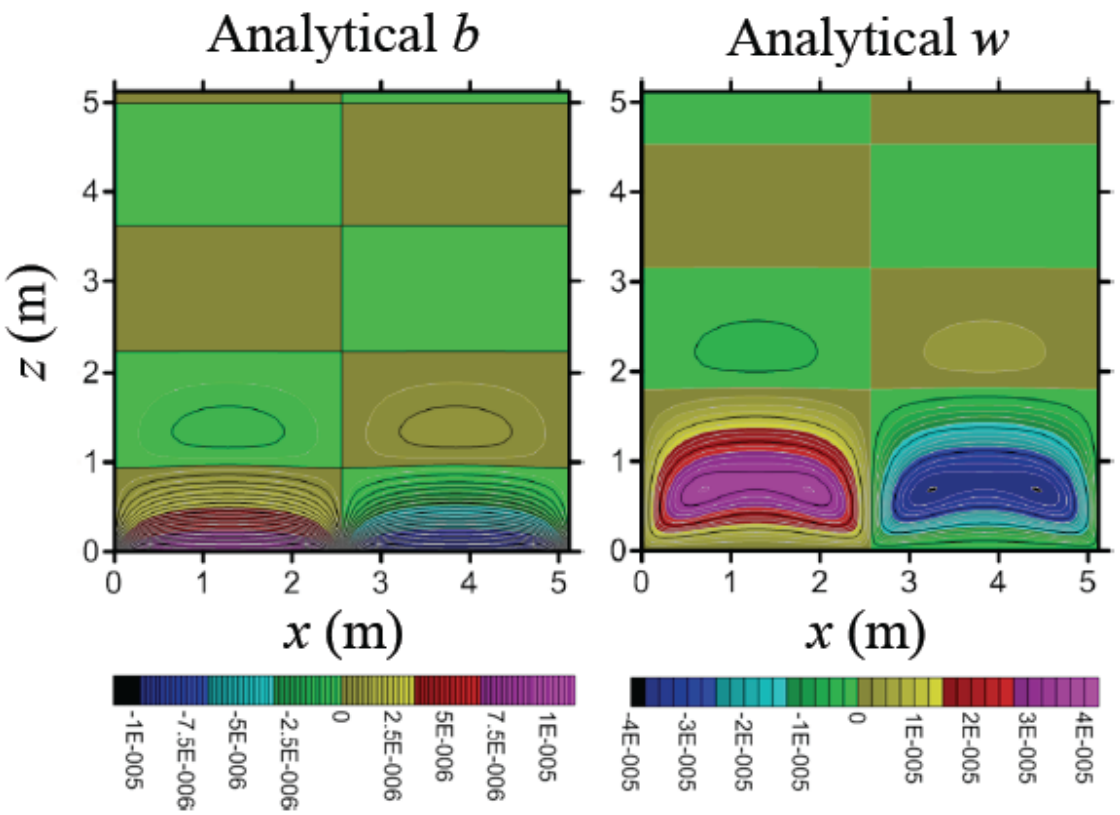

Figure 2. Vertical cross section of the analytical (A-1) buoyancy b and vertical velocity w fields from the first test case. Color bar units are $\mathrm{m\ s^{-2}}$ for b, and $\mathrm{m\ s^{-1}}$ for w.

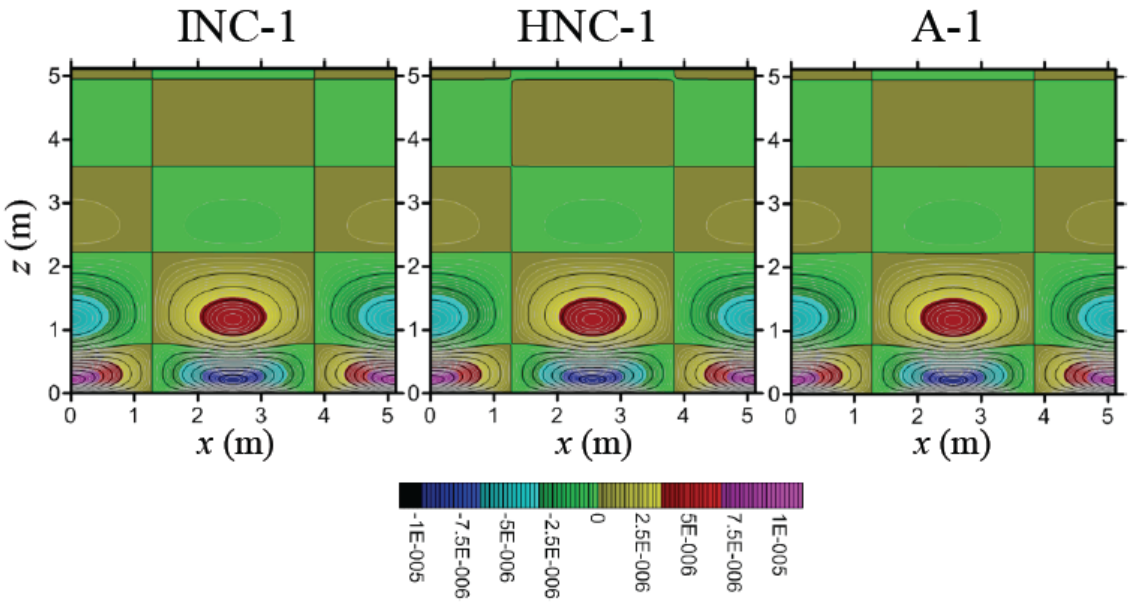

Figure 3. Vertical cross section of u from the first test case. A-1 is the analytical solution. INC-1 is the numerical simulation with inhomogeneous Neumann condition for pressure. HNC-1 is the numerical simulation with the homogeneous Neumann condition for pressure. Color bar units are $\mathrm{m\ s^{-1}}$.

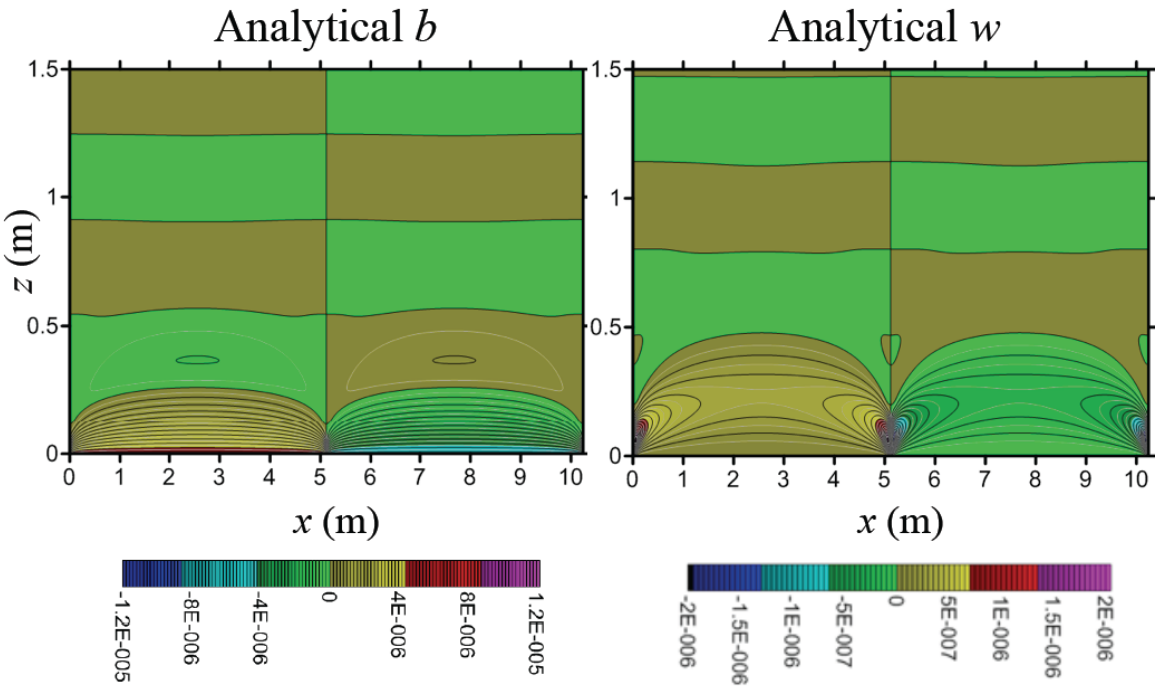

Figure 4. Vertical cross section of the analytical (A-2) buoyancy b and vertical velocity w fields from the second test case. Color bar units are $\mathrm{m\,s^{-2}}$ for b, and $\mathrm{m\,s^{-1}}$ for w.

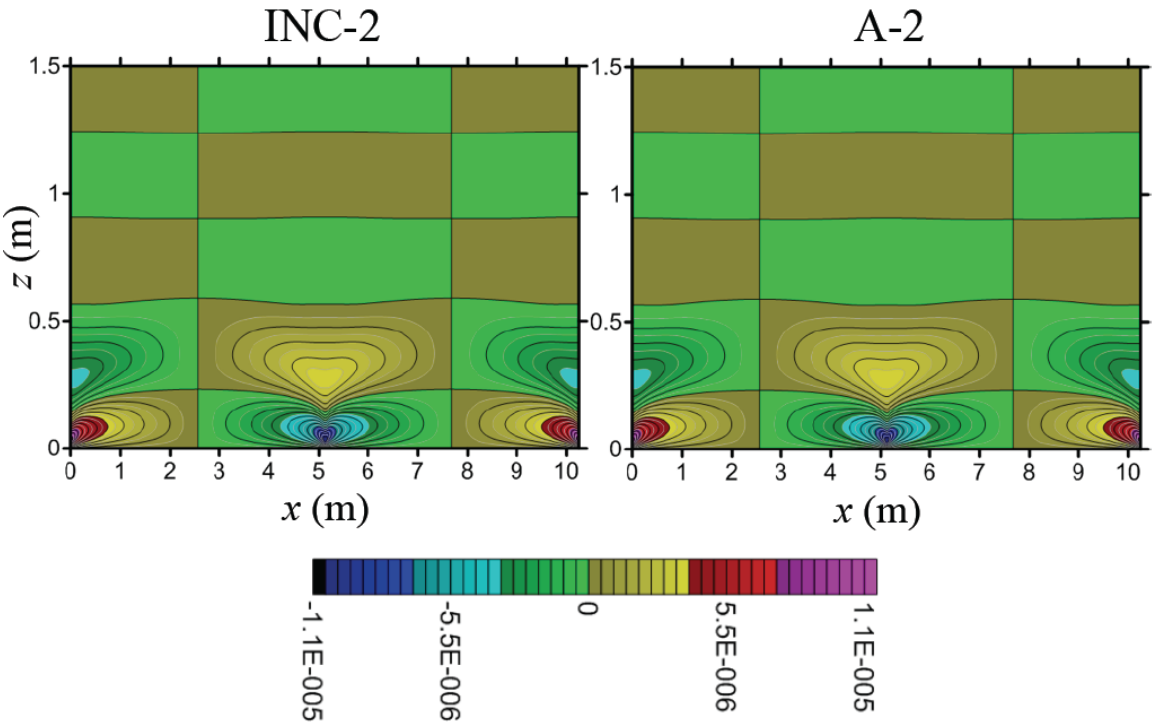

Figure 5. Vertical cross section of u from the second test case. A-2 is the analytical solution. INC-2 is the numerical simulation with inhomogeneous Neumann condition for pressure. Color bar units are m s^{-1}.

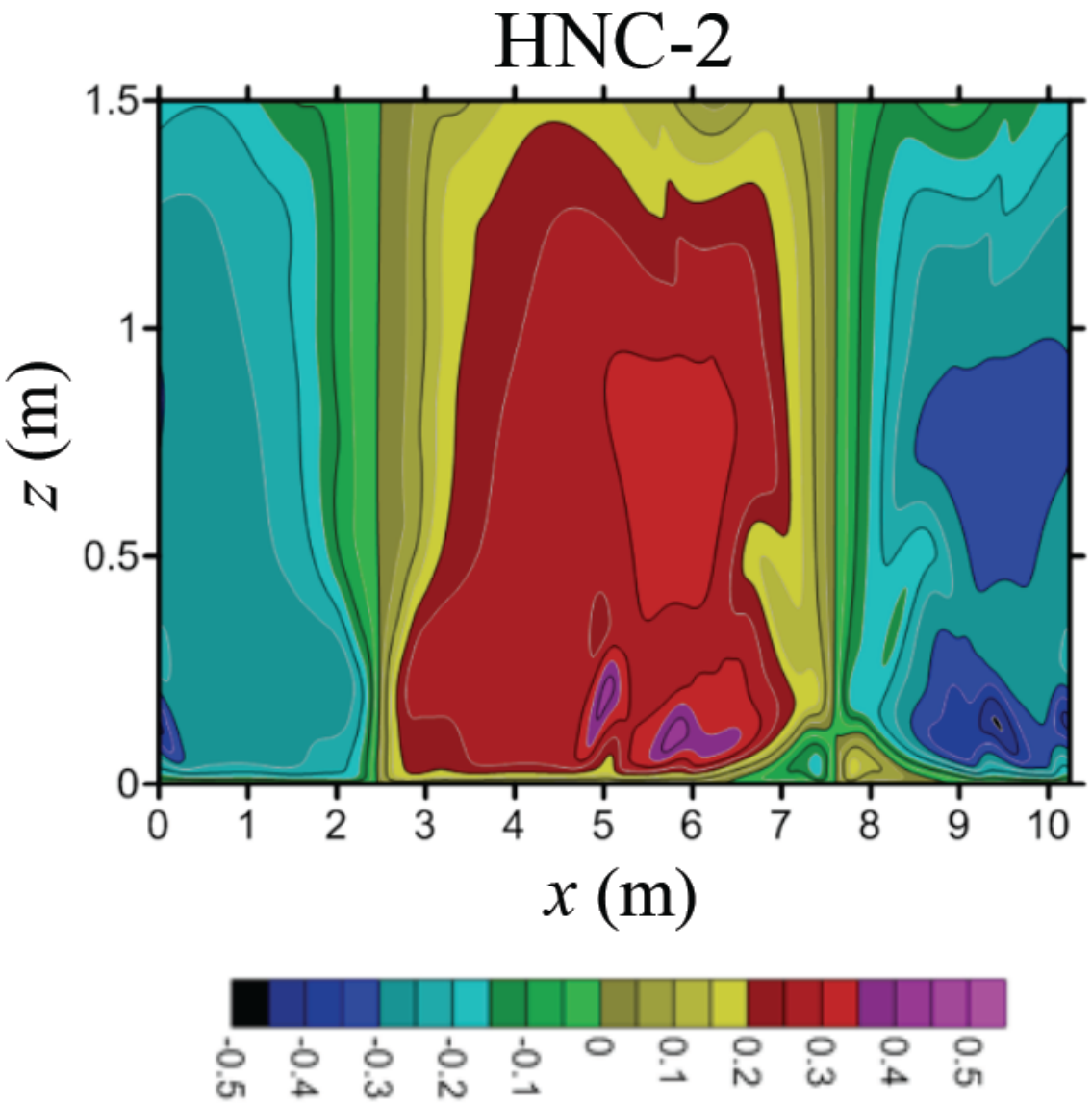

Figure 6. Vertical cross section of u from HNC-2, the numerical simulation with homogeneous Neumann condition for pressure in the second test case. Color bar units are $\mathrm{m\,s^{-1}}$.